



Portable 512 MEMS-Microphone-Array for 3D-Intensity- and Beamforming-Measurements using an FPGA based Data-Acquisition-System

Daniel Ernst¹, Reinhard Geisler¹, Tobias Kleindienst¹, Thomas Ahlefeldt¹, Carsten Spehr¹
¹DLR Institute of Aerodynamics and Flow Technology, Experimental Methods Department
Bunsenstr. 10, 37073 Göttingen, Germany

Abstract

In this paper a portable MEMS-Microphone-Array with integrated Data-Acquisition-System is presented. 512 digital MEMS-Microphones are located in a rectangular box of 17 x 15 x 20 cm. The microphone positions are chosen for sound intensity measurements, but are capable of beamforming as well. Depending on the frequency, these microphones can be used as an array of hundreds of 3D - intensity probes. The acoustic velocity is estimated using a high order three dimensional finite difference stencil to overcome the upper frequency limit of common pp-intensity probes. At low frequencies, pairs with larger spacing are used to reduce the requirement of accurate phase match of the microphone sensors. Additionally a procedure is shown for amplitude and phase calibration of MEMS-Sensors.

All microphone data is collected by an FPGA and send via the UDP-Protocol to any host system for beamforming and intensity calculations in real time or for storing the data to disk.

1 INTRODUCTION

Handheld acoustic arrays are commercially available containing up to 128 microphones. These microphone arrays can be used for beamforming, acoustic intensity measurements or nearfield holography. In order to calculate the acoustic intensity, all these arrays have in common that the microphones are arranged in one or two planes which are placed in parallel to a acoustic radiating surface. Predefined knowledge of the direction of the acoustic intensity is needed. Another common problem is the position tracking of the microphone array itself in the three dimensional space. Camera based systems are available but require the microphone array to stay in the field of view of a stationary camera. The third limitation is the time required to perform

accurate sound intensity measurement. A diffuse sound field may need treatment with acoustic absorbing material and a high spatial resolution requires a long measurement period.

In complex environments like an aircraft cabin under flight conditions the direction of the sound intensity is unknown, stationary tracking cameras are unavailable and a reduction of measurement time is desirable. Therefore a 3D-intensity probe combined with an optical tracking system based on Intel Realsense Cameras was designed to treat these issues. The low weight, small size and low power consumption led to the choice of using MEMS microphones.

There are several studies on using MEMS microphones as an array for example fan measurements [1], beamforming [9], real-time speech acquisition [3] or boundary layer measurements [13]. Most of the digital implementations of MEMS arrays are using FPGAs (Field Programmable Gate Arrays) for the data processing due to their flexibility in programming, scalability regarding sensor count and power consumption.

It is possible to perform a primary calibration of MEMS microphones using the pressure reciprocity [11] or a novel method using photon correlation spectroscopy [10]. Both methods are complex to handle.

There are two options for secondary calibration using a reference microphone. The first method assures that the reference microphone is placed in a tube or cavity smaller than the acoustic wavelength [13] [9] and the second method assumes free field conditions and the device under test and the reference microphone are placed close to each other [8]. For low frequencies the first method is applicable and for high frequencies the second one. In this paper both types are performed.

Kotus et. al. [6] performed the calibration of a MEMS based intensity probe in the free field without a calibration of individual frequency response functions.

The next step in measuring the sound intensity is the calculation of the acoustic particle velocity [2]. A PP-probe uses the 2-point finite difference stencil between the microphones to estimate the spatial derivation of the acoustic pressure field.

Wiederhold et. al. [14] and Lawrence et. al. [7] extended these formulations to a high order finite difference scheme in three dimensions. We will use these methods to estimate the acoustic intensity vector in section 2.2.

2 THEORY AND METHODS

2.1 Hardware Implementation

There are 512 MEMS Microphones of the Type ICS 52000 with an 24-bit integrated AD-conversion distributed over 8 identical PCBs (printed circuit boards). Each PCB contains therefore 64 microphones. The spacing of the PCBs is non-equidistant to provide small spacings for high frequencies and large spacings for low frequencies.

All digital microphone data is time synchronized collected at a sampling frequency of 48 kHz from an FPGA (Xilinx Artix 7) and transmitted to a GigEx-Ethernet ASIC which implements a full network stack and sends one UDP packet per sample to a host laptop to collect all data. The resulting data rate is ≈ 80 MB/s.

The overall power consumption of the microphone array and the FPGA is approximately $1.8 \text{ A} \cdot 3.3 \text{ V} \approx 5 \text{ W}$. Thus it is possible to use a LiPo battery pack with 56.5 Wh for hand-held measurements of several hours.

Two Intel Realsense Cameras (T265 and D435) are mounted below the microphone array and the pose and depth information is collected from the same host laptop. The pose, containing translation and rotation, is sampled at 200 Hz and the depth images at 30 Hz. The synchronization of the two cameras and the microphone array is done with the hardware time stamps.

2.2 Sound Intensity

According to Fahy [2] the mean sound intensity I in the frequency domain is the cross spectra of the acoustic pressure P and velocity \mathbf{U}

$$\mathbf{I} = \frac{1}{2} \text{Re}(P \cdot \mathbf{U}^*) \quad (1)$$

and by combining equation 1 with the fluid momentum equation in the frequency domain

$$\mathbf{U} = \frac{j}{\omega \rho_0} \nabla P \quad (2)$$

results in

$$\mathbf{I} = \frac{1}{2\omega \rho_0} \text{Re}(jP \cdot \nabla P^*) \quad (3)$$

The acoustic pressure P and its spatial gradient ∇P is estimated using a multidimensional Taylor expansion at every microphone position. A system of linear equation is set up by summing up the expansions and set all the terms proportional to a specific exponent to zero. See Lawrence et. al. [7] for further details.

The overall approximation order M is defined as

$$M = M_x M_y M_z \quad (4)$$

where M_x , M_y and M_z are the orders in the different spatial directions.

We denote $\hat{\mathbf{P}} \in \mathbb{R}^N$ as the complex pressure per microphone in the frequency domain, N as the number of microphones, $\mathbf{y} \in \mathbb{R}^3$ as the position where the acoustic intensity is calculated and $\mathbf{x}_n \in \mathbb{R}^3$ as the n -th microphone position.

With these assumptions four systems of linear equations are formed:

$$\mathbf{w} = \mathbf{A}^{-1} \mathbf{b}, \mathbf{w}_x = \mathbf{A}^{-1} \mathbf{b}_x, \mathbf{w}_y = \mathbf{A}^{-1} \mathbf{b}_y, \mathbf{w}_z = \mathbf{A}^{-1} \mathbf{b}_z \quad (5)$$

where

$$[\mathbf{A}]_{n_1+n_2M_1+M_1M_2n_3,n} = \frac{(y_1 - x_{n,1})^{n_1} (y_2 - x_{n,2})^{n_2} (y_3 - x_{n,3})^{n_3}}{n_x! n_y! n_z!} \quad (6)$$

and

$$[\mathbf{b}]_m = \delta(m) \quad (7)$$

$$[\mathbf{b}_x]_m = \delta(m-1), [\mathbf{b}_y]_m = \delta(m-1-M_1), [\mathbf{b}_z]_m = \delta(m-1-M_1M_2) \quad (8)$$

The acoustic pressure and its spatial derivatives at the point \mathbf{y} are then estimated as follows:

$$P \approx \mathbf{w}^T \hat{\mathbf{P}}, \frac{\partial P^*}{\partial x} \approx \hat{\mathbf{P}}^* \mathbf{w}_x, \frac{\partial P^*}{\partial y} \approx \hat{\mathbf{P}}^* \mathbf{w}_y, \frac{\partial P^*}{\partial z} \approx \hat{\mathbf{P}}^* \mathbf{w}_z \quad (9)$$

Using equation 9 and 3 the acoustic intensity is calculated as follows:

$$\omega \rho_0 \mathbf{I}_x \approx \text{Re}(j \mathbf{w}^T \hat{\mathbf{P}} \hat{\mathbf{P}}^* \mathbf{w}_x) = \text{Re}(j \mathbf{w}^T \mathbf{C} \mathbf{w}_x) \quad (10)$$

$$\omega \rho_0 \mathbf{I}_y \approx \text{Re}(j \mathbf{w}^T \hat{\mathbf{P}} \hat{\mathbf{P}}^* \mathbf{w}_y) = \text{Re}(j \mathbf{w}^T \mathbf{C} \mathbf{w}_y) \quad (11)$$

$$\omega \rho_0 \mathbf{I}_z \approx \text{Re}(j \mathbf{w}^T \hat{\mathbf{P}} \hat{\mathbf{P}}^* \mathbf{w}_z) = \text{Re}(j \mathbf{w}^T \mathbf{C} \mathbf{w}_z) \quad (12)$$

$$(13)$$

Here the cross spectral matrix $\mathbf{C} \in \mathbb{C}^{N,N}$ is introduced as known from classical beamforming and the presented approach can be interpreted as steering on the acoustic intensity. An advantage regarding processing speed compared to classical beamforming is that the steering vectors are independent of the frequency.

2.3 Position tracking and 3D-Model of the environment

If the PP512-MEMS Array is used as a handheld device a position tracking system can be used. This system contains two Intel Realsense cameras that are solidly attached to the microphone array. The Intel Realsense T265 camera estimates the position and orientation at 200 Hz sampling frequency and a three dimensional point cloud is given by the Intel Realsense D435 camera at 30 Hz sampling frequency. This point cloud is then rotated and translated according to the global position retrieved by the pose camera (T265). By using the "open3d" [15] python package voxel downsampling is performed on the resulting point cloud. In addition the method "poisson surface reconstruction" of the "open3d" [15] package is used to create triangle mesh for further visualizations.

3 MEASUREMENTS AND RESULTS

In this paper two different calibration procedures are carried out: cavity and freefield calibration. Both methods are second order calibrations. That means that a device under test (DUT, here the MEMS microphone) is compared to a reference microphone.

3.1 Cavity Calibration

In order to do a cavity calibration, one has to assure that the DUT and the reference microphone are close to each other in a cavity with lengths much smaller than the wavelength.

Here a phase calibrator 51AB from G.R.A.S. is used to calibrate the amplitude and phase between two different MEMS microphones of the type ICS 52000. A reference microphone (G.R.A.S. 1/2") is placed in one side of the calibrator and a cylinder made of aluminium (diameter 1/2", height 15 mm) with a 5 mm drilling in the center is placed in the other side. This adapter cylinder is covered with a rubber film (the drill is not covered) and is placed directly on top of the PCB hole with the MEMS microphone at the opposite side of the PCB (see figure 2).



Figure 1: Intel Realsense D435 depth- (top) and T265 pose- (bottom) camera



Figure 2: Measurement setup of the cavity calibration procedure

The speaker in the phase calibrator is driven with white noise between 50 Hz and 6 kHz. Two measurements for two different MEMS microphones are conducted with a measurement period of 60 seconds. The two transfer function between the reference sensor and the MEMS microphones are estimated using the approach of Welch [12]. In figure 3 the resulting difference in amplitude and phase of the transfer function between two MEMS microphones are shown.

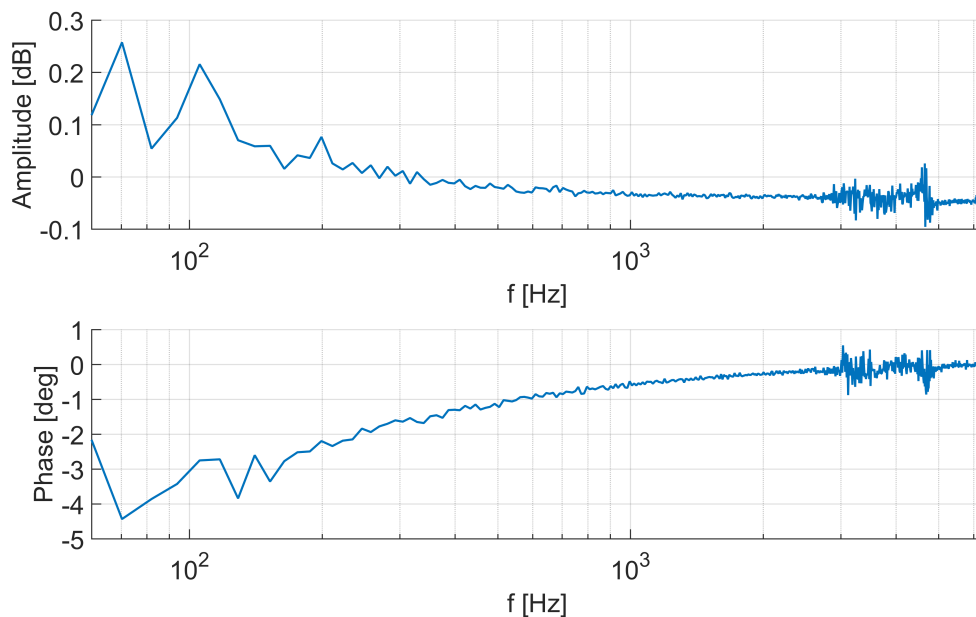


Figure 3: Amplitude and phase difference between two MEMS microphones

The difference in amplitude between 60 Hz and 6 kHz is 0.25 dB at most whereas the difference in phase is up to 4 degree at low frequencies below 100 Hz. Above 1 kHz, the measured phase differences between two MEMS microphones is below ± 1 degree.

3.2 Farfield Calibration

A calibration in the free field was carried out in an anechoic room. During the measurements a foam covered windtunnel was present in the anechoic room, which limits the free field condition. Nevertheless a speaker was placed approximately 1.5 m above the non-reflective ground. The reference microphone (G.R.A.S. 1/2" freefield) and the MEMS microphone array were placed in 2 m distance to the speaker as close (≈ 12.7 mm) as possible to each other (figure 6).

In figure 4 the difference in amplitude and phase between the reference microphone and a MEMS microphone is shown. The amplitude is normalized at 1 kHz and is within ± 2 dB from 50 Hz to 8 kHz and within ± 1 dB from 70 Hz up to 5 kHz. The difference in the phase is within ± 60 degree from 50 Hz to 7 kHz.

3.3 Influence of MEMS-Array on the acoustic field

Due to the size of the PP512 MEMS array ($\approx 0.2 \times 0.2 \times 0.2$ m) which is much larger than the wavelength at 6 kHz (≈ 0.06 m) the PCBs might have an influence on the acoustic field itself. Therefore a reference microphone was placed in the center of PP512 MEMS array (see figure 7) and again a speaker is placed in 2 m distance in an anechoic room. The speaker is driven by white noise. In the next measurement the PP512 MEMS array is removed and only the reference

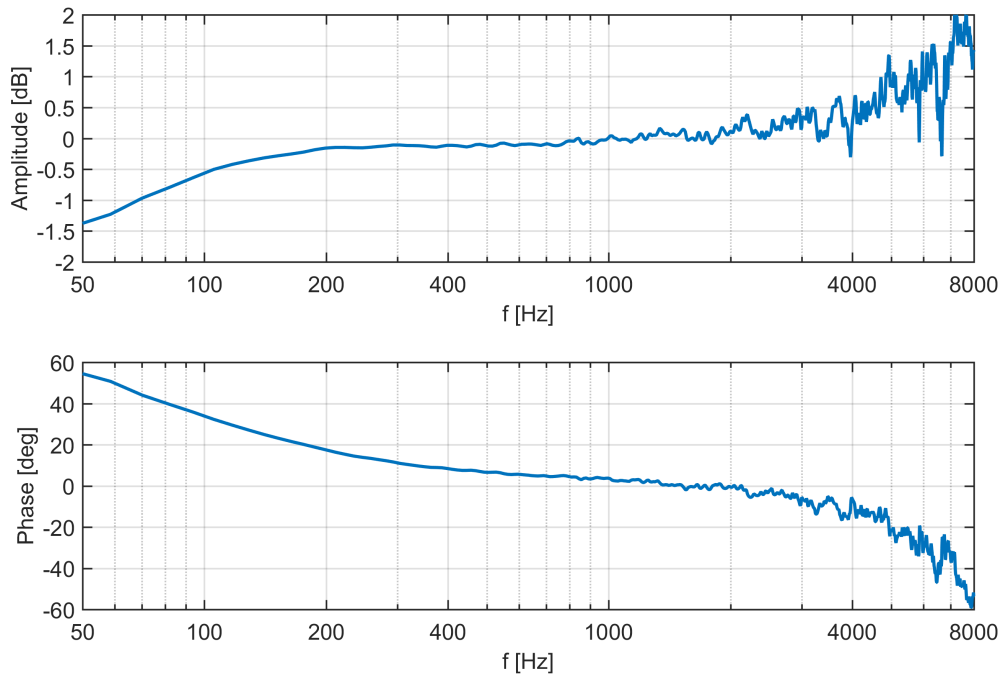


Figure 4: Amplitude and phase difference between a MEMS and a reference microphone (G.R.A.S. 1/2" freefield).

microphone is left. These two measurements are compared regarding the amplitude spectrum of the reference microphone (see figure 5). Up to 3 kHz the difference in amplitude is less than ± 2 dB. Above 3 kHz the difference increases up to 8 dB and thus the influence of the presence of the PP512 MEMS array cannot be neglected.

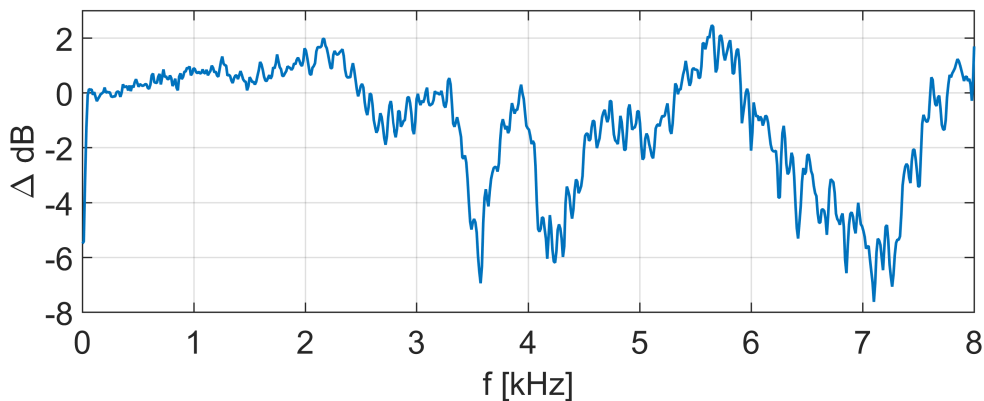


Figure 5: Difference in the amplitude spectrum of the reference microphone with and without the presence of the MEMS microphone (see figure 7).



Figure 6: Measurement setup of the free field calibration procedure.

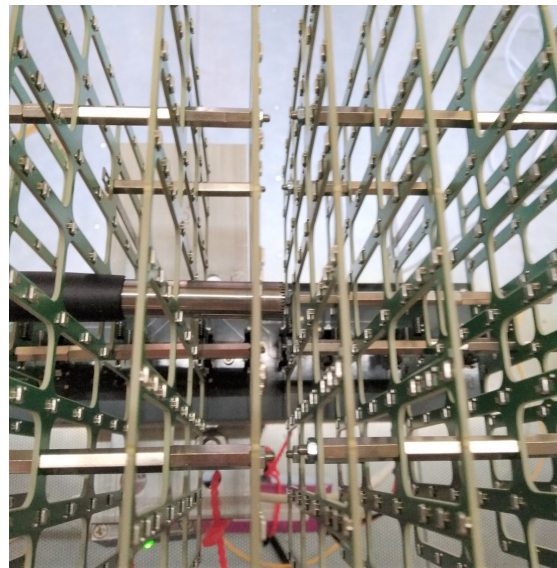


Figure 7: Measurement setup to measure the influence of the PP512 MEMS array on the acoustic field with a reference microphone.

3.4 Comparison to 3D-PP Probe

In this section the PP512 MEMS array is compared to a classical intensity probe from G.R.A.S. of the type 50VI-1. Both probes were placed again 2 m in front of the loudspeaker in an anechoic room. The speaker was driven by white noise and two different measurements were carried out. In figure 10 the acoustic intensity normalized at 1 kHz is shown for both, the classical pp-probe and the PP512 MEMS array. The acoustic intensity was calculated according to section 2.2 and position of the virtual intensity probe was chosen to the exact location of the pp-probe. No phase or amplitude correction was performed. Between 200 Hz and 1.5 kHz the difference in acoustic intensity is less than 1 dB. Below and above this frequency range the acoustic intensity estimated by the PP512 MEMS array is up to 8 dB higher than the estimation of the pp-probe.

3.5 Aircraft Cabin - Dornier 728 ground demonstrator

The last measurement in this paper is carried out in an aircraft cabin demonstrator with integrated shakers behind lining to simulate the acoustic environment inside a real aircraft ([5],[4]). A time signal recorded during flight inside the cabin of an Airbus A320 was used to drive the shaker. As described in section 2.3 the tracking system was used to record the position and orientation of the PP512 MEMS array as well as a point cloud which is converted to a 3D-Model. In figure 11 the 3D-Model and the camera position is shown for one measurement. The quality of the 3D-Model could be improved a lot with the given information, but is not in the field of interest of the authors. Nevertheless a 3D-Model and a position estimation of the hand-held PP512 MEMS array is necessary to have a useful interpretation of the three dimensional acoustic intensity quantities.



Figure 8: Measurement setup to measure the acoustic intensity with a PP-probe.

Figure 9: Measurement setup to measure the acoustic intensity with the PP512 MEMS array.

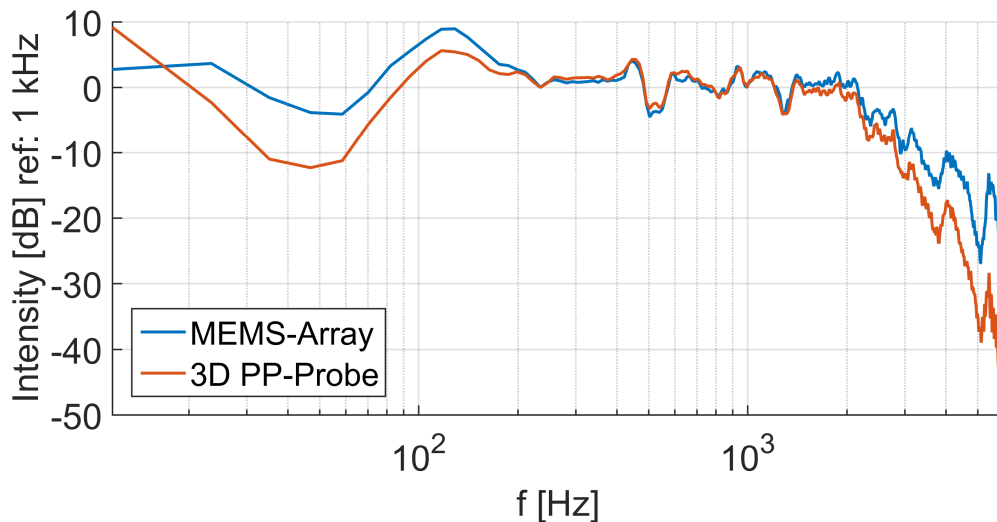


Figure 10: Acoustic intensity normalized at 1 kHz for the measurement setup in figure 8 and 9

Again the acoustic intensity is calculated according to section 2.2 at 343 positions inside the array for each timeblock of 42.66 ms and for each narrow band frequency. Each timeblock is associated with the position and orientation given by the position tracking system at the center time of the timeblock. Assuming a maximum velocity of array movement of 0.5 m/s the accuracy of the acoustic intensity mapping is in the order of 1 cm and the acoustic frequency is shifted due to the doppler effect by at most 0.15 %. The resulting data has a high spatial and non-equidistant resolution. A voxel downsampling approach is performed to reduce the data size as well as complexity and reduces the required averaging time of classical pp-probe measurements. Voxel downsampling means that an equidistant grid of 60 mm resolution is created and all the scattered position data is averaged at the nearest grid point. In figure 12 the resulting acoustic intensity is shown for three different 3rd octave bands (1, 2 and 4 kHz) measured with the PP512 MEMS array near the lining of the aircraft cabin at $x = -0.4$ m.

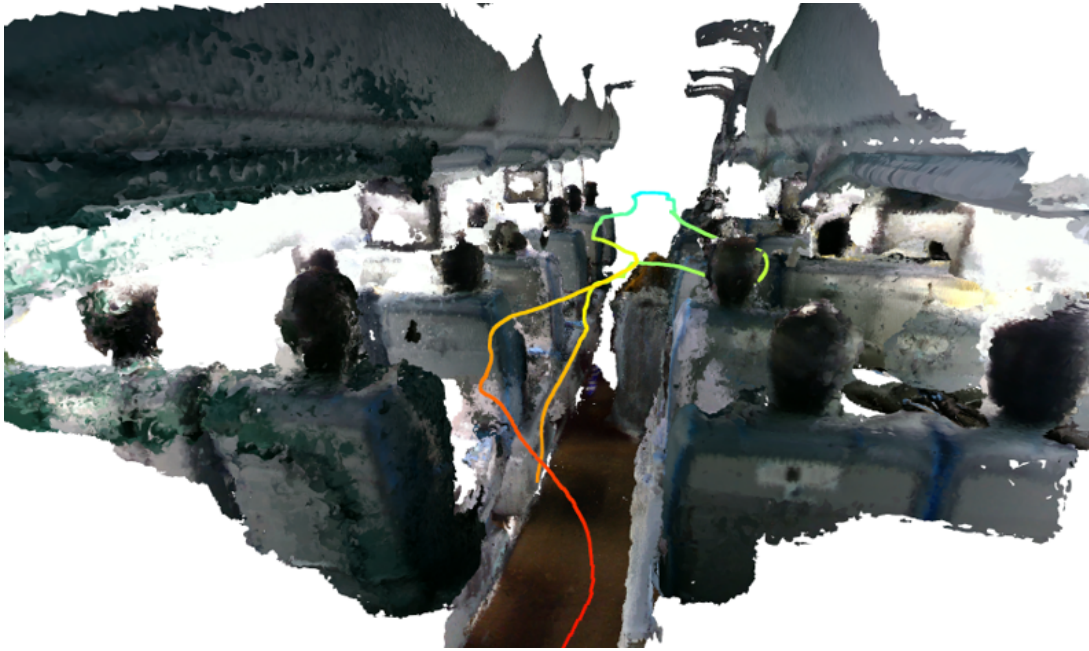


Figure 11: 3D-Model and path of the camera in the Dornier 728 ground demonstrator.

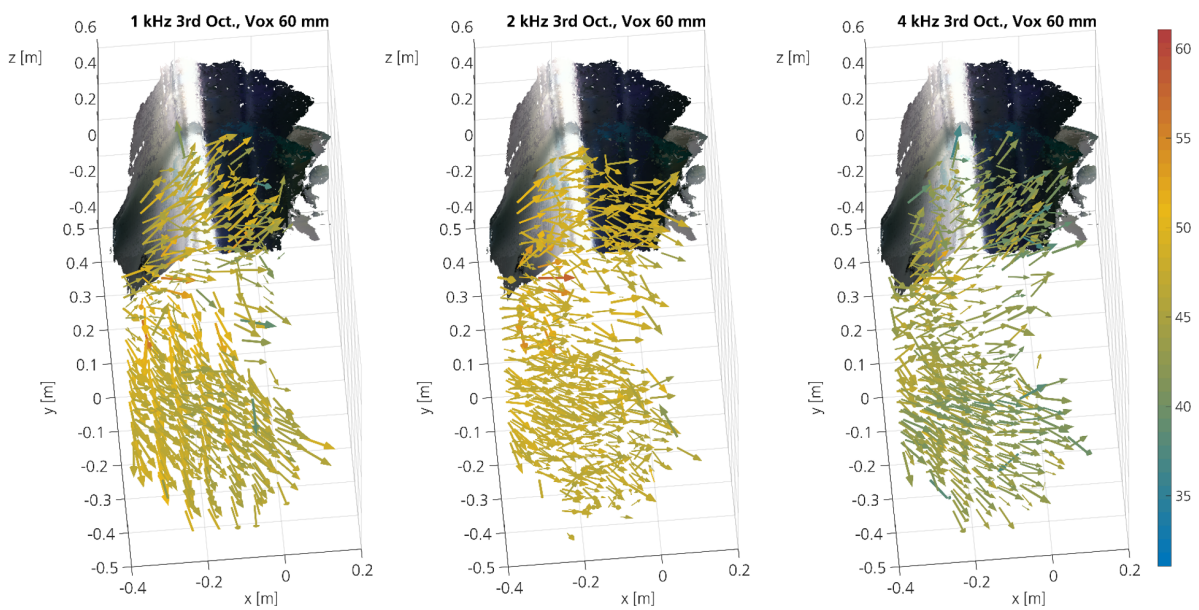


Figure 12: Acoustic intensity level at the 3rd octave bands 1, 2 and 4 kHz and a voxel down-sampling of 60 mm.

4 CONCLUSION

The use of MEMS as acoustic intensity probe was shown for an arbitrary microphone layout and implemented using a FPGA based data acquisition system. It was shown that the estimation of the acoustic intensity can be seen as a kind of beamformer where the steering vectors are the weighting factors of the Taylor expansion. A tracking system consisting of Intel Realsense cameras was shown and found out to be very robust against fast movements and a position accuracy below 1 mm at laboratory test in a limited field of movement of 30 cm. The calibrations procedures for MEMS microphones are time consuming and requiring a precise handling regarding positioning of the calibrator on the sound hole of the MEMS microphones. Nevertheless for frequencies below 6 kHz a commercially available phase calibrator can be used to perform the relative calibration of MEMS microphones to each other regarding phase and amplitude. An absolute calibration of the amplitude and phase can be done by a measurement in the free field and comparison with a reference microphone. The influence of the microphone array geometry on the acoustic field is not negligible and above 3 kHz the change in amplitude can increase up to 8 dB. But even without any frequency response calibration of the MEMS microphones the acoustic intensity can be measured in high spatial resolution and in complex environments such as an aircraft cabin without any preinstallations.

References

- [1] L. del Val, A. Izquierdo, J. J. Villacorta, and L. Suárez. “Using a planar array of MEMS microphones to obtain acoustic images of a fan matrix.” *Journal of Sensors*, 2017, 1–10, 2017. doi:10.1155/2017/3209142.
- [2] F. Fahy. *Sound Intensity*. CRC Press, 1995. ISBN 0419198105. URL https://www.ebook.de/de/product/6432207/frank_university_of_southampton_fahy_sound_intensity.html.
- [3] I. Hafizovic, C.-I. C. Nilsen, M. Kjølerbakken, and V. Jahr. “Design and implementation of a MEMS microphone array system for real-time speech acquisition.” *Applied Acoustics*, 73(2), 132–143, 2012. doi:10.1016/j.apacoust.2011.07.009.
- [4] C. S. Judith Kokavecz. “Microphone array technology for enhanced sound source localisation in cabins.” *AIA-DAGA 2013 Merano*, 2013.
- [5] C. S. Judith Kokavecz, Lasse Seemann. “Akustisch fliegen ohne abzuheben.” *DAGA 2012*.
- [6] J. Kotus and G. Szwoch. “Calibration of acoustic vector sensor based on MEMS microphones for DOA estimation.” *Applied Acoustics*, 141, 307–321, 2018. doi:10.1016/j.apacoust.2018.07.025.
- [7] J. S. Lawrence, K. L. Gee, T. B. Neilsen, and S. D. Sommerfeldt. “Higher-order estimation of active and reactive acoustic intensity.” Acoustical Society of America, 2017. doi:10.1121/2.0000610.
- [8] C. Mydlarz, C. Shamoan, M. Baglione, and M. Pimpinella. “The design and calibration of low cost urban acoustic sensing devices.” 2015.

- [9] S. Orlando, A. Bale, and D. Johnson. “Design and preliminary testing of a MEMS microphone phased array.” In *Proceedings on CD of the 3rd Berlin Beamforming Conference, 24-25 February, 2010*. 2010. ISBN 978-3-00-030027-1. URL <http://bebec.eu/Downloads/BeBeC2010/Papers/BeBeC-2010-21.pdf>.
- [10] B. Piper, T. Koukoulas, R. Barham, and R. Jackett. “Measuring mems microphone free field performance using photon correlation spectroscopy.” 2015.
- [11] R. P. Wagner and S. E. Fick. “Pressure reciprocity calibration of a MEMS microphone.” *The Journal of the Acoustical Society of America*, 142(3), EL251–EL257, 2017. doi:10.1121/1.5000326.
- [12] P. Welch. “The use of fast Fourier transform for the estimation of power spectra: A method based on time averaging over short, modified periodograms.” *IEEE Transactions on Audio and Electroacoustics*, 15(2), 70–73, 1967. doi:10.1109/tau.1967.1161901. URL <http://dx.doi.org/10.1109/TAU.1967.1161901>.
- [13] R. White, J. Krause, R. D. Jong, G. Holup, J. Gallman, and M. Moeller. “MEMS microphone array on a chip for turbulent boundary layer measurements.” In *50th AIAA Aerospace Sciences Meeting including the New Horizons Forum and Aerospace Exposition*. American Institute of Aeronautics and Astronautics, 2012. doi:10.2514/6.2012-260.
- [14] C. P. Wiederhold, K. L. Gee, J. D. Blotter, S. D. Sommerfeldt, and J. H. Giraud. “Comparison of multimicrophone probe design and processing methods in measuring acoustic intensity.” *The Journal of the Acoustical Society of America*, 135(5), 2797–2807, 2014. doi:10.1121/1.4871180.
- [15] Q.-Y. Zhou, J. Park, and V. Koltun. “Open3D: A modern library for 3D data processing.” *arXiv:1801.09847*, 2018.